



**HAL**  
open science

## Statistical investigation of different analysis methods for chloride profiles within a real structure in a marine environment

Inès Othmen, Stéphanie Bonnet, Franck Schoefs

► **To cite this version:**

Inès Othmen, Stéphanie Bonnet, Franck Schoefs. Statistical investigation of different analysis methods for chloride profiles within a real structure in a marine environment. *Ocean Engineering*, 2018, 157, pp.96 - 107. 10.1016/j.oceaneng.2018.03.040 . hal-01923540

**HAL Id: hal-01923540**

**<https://hal.science/hal-01923540>**

Submitted on 26 Nov 2018

**HAL** is a multi-disciplinary open access archive for the deposit and dissemination of scientific research documents, whether they are published or not. The documents may come from teaching and research institutions in France or abroad, or from public or private research centers.

L'archive ouverte pluridisciplinaire **HAL**, est destinée au dépôt et à la diffusion de documents scientifiques de niveau recherche, publiés ou non, émanant des établissements d'enseignement et de recherche français ou étrangers, des laboratoires publics ou privés.



27  
28  
29  
30  
31  
32  
33  
34  
35  
36  
37  
38  
39  
40  
41  
42  
43  
44  
45  
46  
47  
48  
49  
50  
51  
52  
53  
54  
55

1. Introduction

Chloride penetration into concrete can cause irreversible damage within reinforced concrete structures, predominantly corrosion damage, when chloride content at the surface of reinforcement bars reaches a certain threshold level. Steel corrosion initiation is then a key indicator for the estimation of service life. The risk of corrosion damage is higher in a marine environment because of significant humidity and chloride contents in both seawater and air. Consequently, the corrosion of engineering structures is more severe in coastal areas than inland locations (Guo et al., 2015). Chloride profile analysis, is therefore, an important tool for service life predictions of structures and inspection/maintenance/repair action scheduling (Bastidas-Arteaga et al., 2011; de Rincón et al., 2004). Recent studies have highlighted the spatial variability of chloride-induced reinforced concrete corrosion with an impact on infrastructure network maintenance optimization (O'Connor and Kenshel, 2013). In the following, the focus is on total chloride content because, firstly, measurement methodology is not subject to debate (Bonnet et al., 2017) and, secondly, because it is the key parameter for already available maintenance optimisation methods.

Chloride profile analysis is therefore essential. Profiles are better assessed when different factors like concrete properties (Tadayon et al., 2016) and period of exposure (Mangat and Molloy, 1994, Tamimi et al., 2008) are taken into account. Exposure (above sea level: atmospheric and splashing zones, and under sea level: tidal and immersed zones) and environmental conditions (temperature, relative humidity, wind, orientation...) are also important factors in affecting the durability of concrete and in shortening the life span of structures. Many studies have shown that tidal and splash zones drive the most severe conditions as regards chloride ingress and steel corrosion of concrete in comparison with atmosphere and immersed zones (Valipour et al., 2013). Li and Shao (2014) conclude that immersed zones allow for a service life 1.6 to 3.9 times longer than splash zones, whatever the binding isotherm considered. Furthermore, in marine exposure conditions, chloride ions can penetrate into concrete through multiple mechanisms including diffusion, adsorption, permeation and surface deposit of airborne salts (Hilsdorf and Kropp, 2004). Although chloride ingress within concrete involves many mechanisms, it is widely accepted that diffusion is the primary mechanism (Pang and Li, 2016). Hence, chloride ingress can be modelled by the empirical Fick's diffusion model. Besides, The Fick's model is used by engineers and researchers to deal with in situ data (see references on table 1) and recommended by codes like Fédération International du Béton (2006) for its simplicity and its capacity of being adapted to different exposure cases.

56 Indeed, a comparison of an oversimplified model to an improved model shows that both yields to similar results  
57 (Nguyen et al., 2017) and fairly well predict the chloride ingress in a Portland cement (up to 100 years) (Luping  
58 and Gulikers, 2007). Moreover, a long-term monitoring on real concrete structures exposed to environmental  
59 conditions makes the empirical Fick's model adapted for durability design (Li et al., 2015).

60 Then, many studies have been devoted to the measurement of chloride ingress within real structures like decks,  
61 piles, offshore platform or concrete specimens, in a marine environment with different exposure conditions  
62 (Table 1). The chloride profiles obtained (often) have the shape of a bell with a chloride content, which increases  
63 from the concrete surface to a certain depth where a maximum content, noted  $C_{peak}$  in Table 1, is reached and  
64 then decreases as depth increases. This is accounted for by (Andrade et al., 1997) as "concrete surface skin  
65 effect". In the studies reported in Table 1, the approach commonly used to estimate both surface content  $C_s$  and  
66 diffusion coefficient  $D$  come from the fitting of the Fick's second law to in-situ values of experimental chloride  
67 profiles. This regression beginning at  $C_{peak}$  provides  $C_s$  and  $D$  simultaneously.

68 It should be noted that the value of  $C_{peak}$  varies from 0.0014  $\text{kg}_{\text{Cl}}/\text{kg}_{\text{concrete}}$  (Pang and Li, 2016) to 0.013  
69  $\text{kg}_{\text{Cl}}/\text{kg}_{\text{concrete}}$  (Chalee et al., 2009).  $C_{peak}$  can also start at 0 mm (Chalee et al., 2009; de Rincón et al., 2004),  
70 around 10 mm (Medeiros-Junior et al., 2015; Pang and Li, 2016; Thomas and Matthews, 2004), and at 20 mm or  
71 30 mm (de Rincón et al., 2004). The depth may vary in relation to concrete quality, exposure conditions and  
72 structure orientation. Some values of  $D$  obtained vary between  $0.27 \times 10^{-12} \text{ m}^2/\text{s}$  (da Costa et al., 2013) and  
73  $5.13 \times 10^{-12} \text{ m}^2/\text{s}$  (Medeiros-Junior et al., 2015).

74 Among key parameters and phenomena (quality of concrete, exposure conditions and orientation) affecting  
75 structure service life, exposure conditions are the focus of this research. The present paper, indeed, reports the  
76 experimental investigation carried out on a 28-years old beam made from the same concrete composition and on  
77 which all the chloride profiles are measured on the same horizontal line (coring is performed on the same line  
78 along the beam). Moreover, the studied beam is located in a splash zone influenced by two local microclimates  
79 (both beam exposures are detailed in §2.1). The present study also provides a significant number of chloride  
80 profiles in accordance with (Medeiros-Junior et al., 2015), who underline the significance of the number of  
81 samples as a direct benefit to achieve precise statements. Furthermore, De Vera G. et al. (2015) highlighted that  
82 to assign reliable values for  $C_s$  it is only possible on the basis of experimental chloride profiles obtained with the  
83 similar concrete composition and in similar locations. As for  $D$ , the sensitivity analysis realised by Li et al.

84 (2009) shows that the achieved reliability of design is rather sensitive to the mean of  $D$  values as well as the  
 85 cover thickness. It is thus necessary to evaluate  $D$  accurately.

86 These data form a substantial high value data base to improve the scientific documented knowledge library for  
 87 concrete subject to XS3 class environmental exposure according to the NF EN 206-1 standard. The objective of  
 88 this research is to address the problem of the determination of  $C_s$  that usually results from the chloride content  
 89 reduction at the concrete surface (Song et al., 2008). So, the variation of the position where  $C_{peak}$  is measured  
 90 appears to constitute a possible alternative route for study.

91 Thus, this paper provides an important data base of chloride measurements done on the same beam with reduced  
 92 settings like concrete composition, location, marine environment and tidal height that were all the same for 30  
 93 core samples. Indeed, approximately 600 chloride measurements were carried out to highlight the observations  
 94 and comments done hereafter. On a comparable data, it is possible, on the one hand, to underline the variability  
 95 of the raw data of chloride profiles and, on the other hand, the variability of  $C_s$  and  $D$  along the beam once the  
 96 raw data was processed by Fick's second law solution. This work, as far as we know, has never been done on so  
 97 many data.

98 Since very numerous comparable data are available it led us to review the generic treatment used by some  
 99 authors to deal with chloride profiles to determine  $C_s$  and  $D$  (Chalee et al., 2009; da Costa et al., 2013; Pang and  
 100 Li, 2016). This treatment was compared to the individual treatment called reference case in this paper which is  
 101 more time consuming than the previous treatment.

102 Accordingly, the paper is structured as follows:

- 103 - Experimental investigation of the studied structure.
- 104 - Experimental chloride profile fitting methodology based on three sets of analyses depending on the  
 105 chloride maximum content position and using Fick's second law to assess  $C_s$  and  $D$ .
- 106 -  $C_s$  and  $D$  results presentation for the three sets of analyses. The focus is made on the reference case to  
 107 derive the statistical distribution and the covariance.

Table 1: Peak values of total\*\* chloride content and diffusion coefficient of concrete structures and specimens exposed to a marine environment

Reference	Structure	Exposure conditions	Construction period	Investigation period (year)	Number of samples	Peak position* (mm)	$C_{peak}$ * (kg/kg)	$D$ * ( $10^{-12}$ m <sup>2</sup> /s)
(de Rincón et al., 2004)	Bridge pier	Above the sea level	1962-1963	33	-	Around 20-30	0.0028	-
			1938	64			0.0025	

	bridge		1986		11		0	0.0018	
(da Costa et al., 2013).	Offshore oil platform	Wetting drying cycles			25	35	Around 10-20	0.0029 : 0.0051	0.27 : 1.6
(Chalee et al., 2009)	Cube specimens (in sea water)	Two wet dry cycles of sea water daily	-		5	-	0 mm	0.013	1.65
(Pang and Li, 2016)	Pile wharf structure	splash zone	between 1971 and 2008		36	8/pile 14 piles tested	Between 0 and 10	0.0046	0.35
(Medeiros-Junior et al., 2015)	Offshore platform	splash zone	1976		29	3 layers/ point of investigation	10	0.007	5.13
(Thomas and Matthews, 2004)	Cube specimens (in sea water)	Tidal zone	-		1, 2 and 10	-	around 7.5 -10	0.0038 : 0.006	-
(Pritzl et al., 2015)	Deck bridge	deicing salt environment	Between 1992 and 1995		16	4 locations	10	0.0059	2
(Tadayon et al., 2016)	Cube specimens (in sea water)	Tidal zone	-		4.17 (=50 months)	-	2.5	0.006 : 0.0091	2:4.2
(Cramer et al., 2002)	bridge	Marine breeze	-		40 to 60	-	-	0.0073 : 0.003	0.41 : 1.71
(Kenshel, 2009)	pier	Atmospheric zone	1980		27	45	Between 10 and 25 mm	0.0004 : 0.0013	0.098 : 0.72

108 \* Peak position is the position within the sample where the maximum chloride content ( $C_{peak}$ ) is measured. When information are missing to  
109 convert  $C$  and  $D$  into  $kg/kg$  and  $m^2/s$ , respectively, we considered Cement concentration =  $350kg/m^3$  and concrete bulk density =  $2500kg/m^3$

110 \*\*except for Medeiros-Junior et al., 2015 where only free chloride content is measured

## 111 2. Experimental investigation of the studied structure

### 112 2.1. Test Area

113 Harbour infrastructures, especially energy-related ones, are important components of the transportation system in  
114 coastal areas. We, therefore, focus on the coal terminal of the test area. The coal terminal is located within the  
115 industrial and port activity area, which includes many specialised facilities near the city of Saint-Nazaire  
116 (France). The coal terminal, which is one of the largest thermal power stations in Europe, is used for the import  
117 and then the transportation of coal by inland waterways to support French power supply.

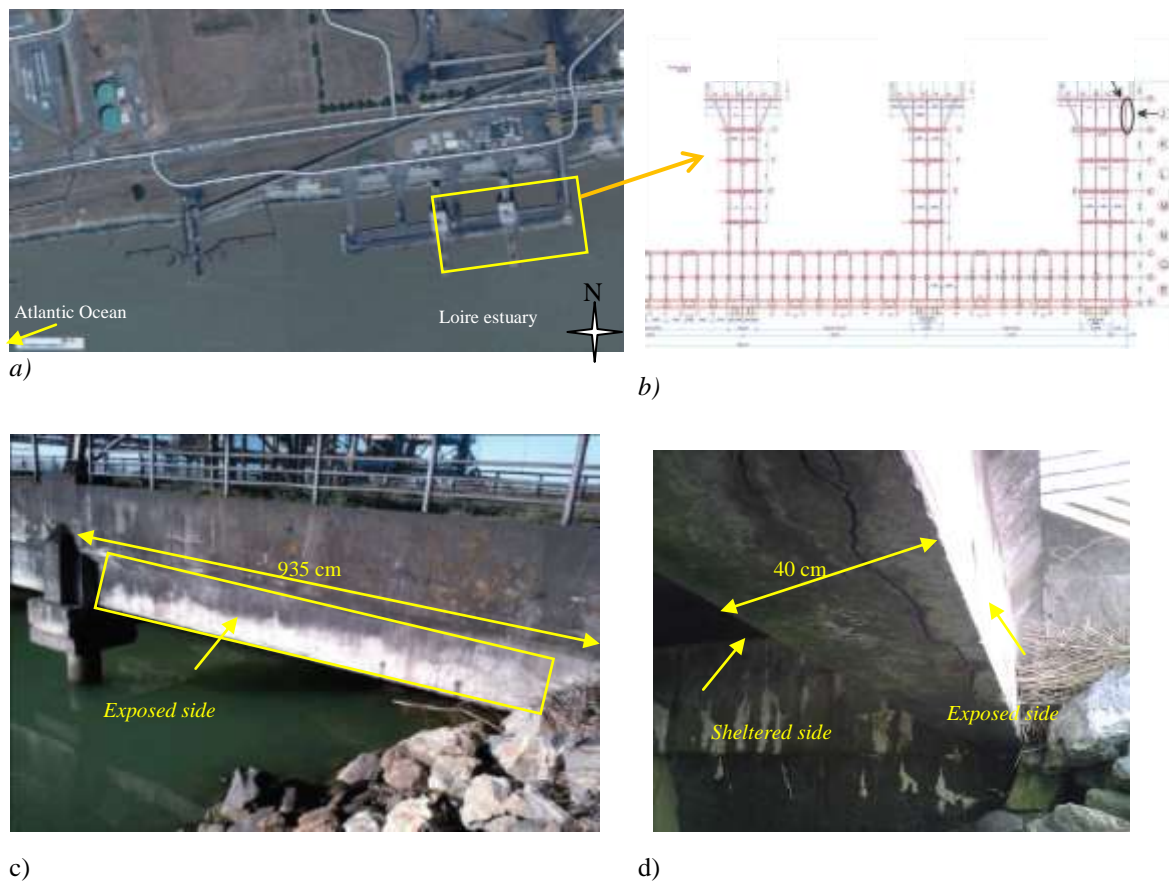
118 The coal terminal (Fig. 2a), built between 1981 and 1983, consists of five bridge piers (54.5m in length \*9.8 m  
119 in width each) giving access to an unloading platform (246.4 m in length\* 20.7 m in width).

120 For accessibility reasons, the study is conducted on beam J of Pier 5 (Fig. 1b). The beam is 9.35m long and  
 121 0.40m wide. The upstream side, exposed to weather variations, is called “exposed side” (noted ES) whereas the  
 122 protected downstream face being situated in a confined environment is called “sheltered side” (noted SS) (Fig.  
 123 1c and Fig. 1d). Beam J is located in the estuary area of the Loire River less than 7 km from the Atlantic Ocean.  
 124 The beam is situated 5.8 m above sea level, in a splash zone where the bottom of the beam may be in contact  
 125 with seawater when tidal coefficients are high (roughly 2 days/month). The climatic data, including temperature  
 126 (T), relative humidity (RH) and wind speed, cumulative rainfall and the atmospheric pressure (P), have been  
 127 recorded by the French Government weather station<sup>1</sup> near the Saint-Nazaire harbour (Table 2). Temperature  
 128 mean maximal and minimal values are 16.9°C and 8.7°C, respectively, with high relative humidity (>80%).

Table 2: Climatic data of the beam surrounding environment

	Mean max T [°C]	Mean min T [°C]	Mean RH [%]	Maximal Wind speed [km/h]	Cumulative Rainfall [mm]	Max rainfall per 24h [mm]	Max P [hPa]	Min P [hPa]
Mean value (between 1981 and 2011)	16.9	8.7	>80%	133.3	788.6	61.8	961.6	1088

129



<sup>1</sup> <http://www.infoclimat.fr/stations-meteo/climato-moyennes-records>.

Fig. 1: Coal terminal a) aerial view b) sketch of bridges 3,4 and 5 c) Picture of beam J d) Exposed and sheltered sides of beam J

130 2.2. Concrete composition

131 When studying the existing documentation from the coal terminal, we find some data available about the  
 132 concrete. It is a Portland cement where clinkers make up more than 90% of the cement and secondary  
 133 constituents shall not exceed 5%. The cement has also a strength class of 45 MPa . The aggregates used are sand  
 134 0/6 and gravel 5/10 and 10/25. The cement content of 350kg/m<sup>3</sup> is specified but not aggregate and water  
 135 contents.

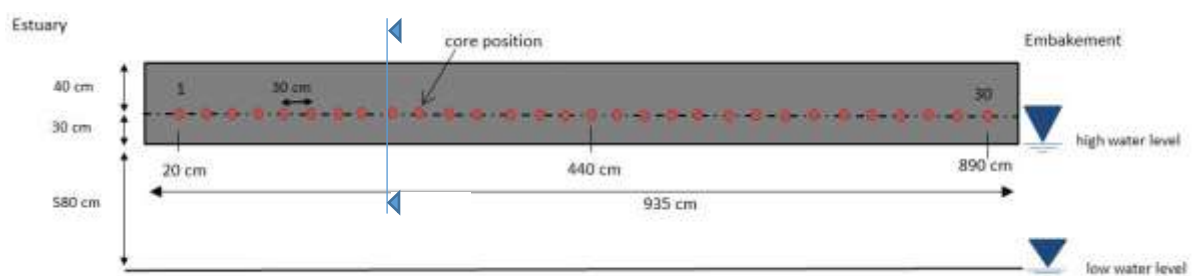
136 Concrete open water porosity and compressive strength are both measured on the central parts of the extracted  
 137 cores that were sawn and rectified to obtain a flat surface (slide Number 3 in Fig. 2c).

138 Concrete cylinders were oven-dried at 60 °C until reaching constant weight. Then they were cooled for 48 h in a  
 139 desiccator at 20 °C before being water saturated to determine their open water porosity (Ben Fraj et al., 2012).

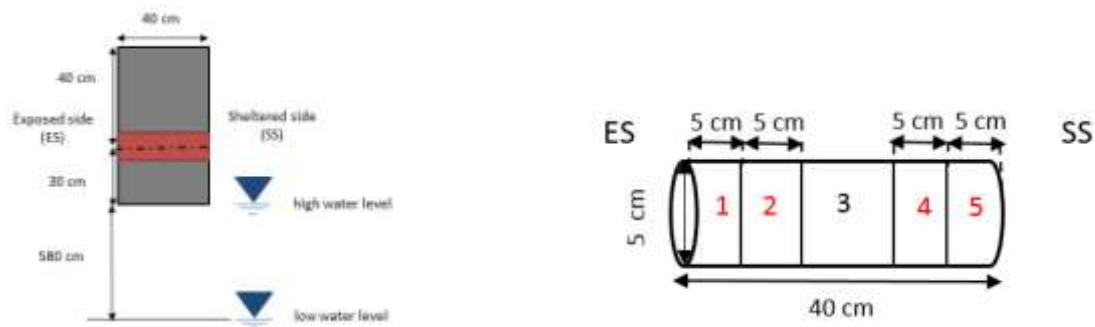
140 The porosity is obtained from five samples with a mean value of 13.7% (min value =11.3% and max value  
 141 =15.9%). The compressive strength is obtained from four 5-cm diameter and 10-cm long samples. The loading  
 142 speed was of 5kN/s. The mean value is 43.5MPa (min value =38.5MPa and max value =48.9MPa).

143 2.3. Experimental investigation for chloride content

144 The extraction of the cylindrical cores took place in 2011 after 28 years of exposure and carried out along a line  
 145 situated 30 cm above the bottom of the beam. Thirty samples have been collected every 30 cm (red dots in Fig.  
 146 2a) and numbered from 1 to 30 from the Loire estuary side to the embankment side of the beam.



a)



b)

c)

Fig. 2: Investigation line a) front view with cores positions b) cross section A-A and c) sample diagram

147 The thirty specimens are cylinders 5 cm in diameter and 40 cm in length. Each core is cut into five slices: slices  
 148 1 and 2 correspond to the exposed side (ES) and slices 4 and 5 to the sheltered side (SS) (Fig. 2c). All are used to  
 149 determine the chloride profiles. Slice n°3 is used for other investigations like porosity and compressive strength  
 150 (§2.2) and for the determination of the initial chloride content (§3.2).

151 The procedure recommended by the RILEM Technical Committee 178-TMC (“Recommendation for analysis of  
 152 total chloride in concrete,” 2006) is followed to obtain the chloride profiles. Slices are grounded first into 5-mm  
 153 thick layers up to a depth of 5 cm (slices 1 and 5 in Fig. 2c) and then into 10-mm thick layers for the remaining 5  
 154 cm (slices 2 and 4 in Fig. 2c). This method makes it possible to monitor the progression of the fitting and to  
 155 assess the peak position on the profile with good accuracy ( $\pm 2.5$  mm), the other parts of the core (# 2 and #4)  
 156 having less impact on the fitting accuracy. For the recovery of powder, grinding is made perpendicularly to the  
 157 top faces of the cylinders using a grinding instrument as recommended by Vennesland (Vennesland et al., 2012).  
 158 The powder is collected and stored in sealed plastic bags. The procedure described below is used to determine  
 159 the total chloride content from concrete powder (Chaussadent and Arliguie, 1999; Vennesland et al., 2012).

160 In order to extract the chloride from the concrete powder samples, 100 ml of nitric acid is added to 5 g of  
 161 grounded concrete powder. The mixture is heated and stirred for 30 min. The solution obtained is then filtered  
 162 into a 250-cm<sup>3</sup> volumetric flask. The chloride content of the filtered solutions is finally determined by  
 163 potentiometric titration using an automatic titrator with 0.05-M silver nitrate (AgNO<sub>3</sub>) as titrant.

### 164 3. Fitting method

#### 165 3.1. Chloride profiles

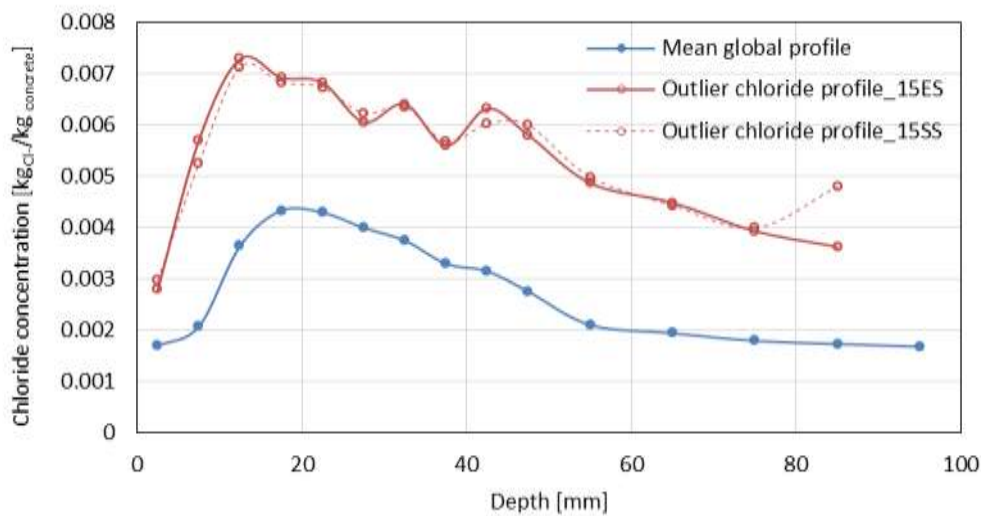
166 The chloride content is plotted as a function of the distance (in mm) from the top surface for both sides (SS and  
 167 ES) to illustrate chloride profiles. Samples are numbered from 1 to 30 as shown in Fig. 2a. 37 workable profiles

168 are thus obtained, which are distributed as follows: 21 profiles from the sheltered side (SS) and 16 profiles from  
 169 the exposed side (ES). The profiles are summarized in Table 3 (cross mark means availability).

170 Missing profiles 9, 11, 12 and 26 correspond to the cores damaged during sampling. Other profiles have also  
 171 been eliminated. Indeed, when plotting chloride concentrations as a function of depth, some profiles present a  
 172 linear trend suggesting the presence of cracks that may trap a significant amount of chloride (**Erreur ! Source**  
 173 **du renvoi introuvable.**—curves with empty markers).

174 Wang et al. (2016) have examined the effects of different crack parameters on the chloride diffusion into  
 175 concrete and have demonstrated that it highly depends on the crack density (represents the amount of cracks), in  
 176 addition to crack width and crack tortuosity.

177 An outlier reveals a very high chloride content in the chloride profile, which should then be discarded. The  
 178 discarded profiles here are 3, 15 17, 20 and 29 on the sheltered side and 3, 6, 7, 8, 9, 15, 17, 20, 22 and 29 on the  
 179 exposed side. 37 profiles are finally processed. The mean global profile, represented as the mean chloride  
 180 content for both sides (mean of the 37 profiles), is given in Fig. 3 (blue solid line).



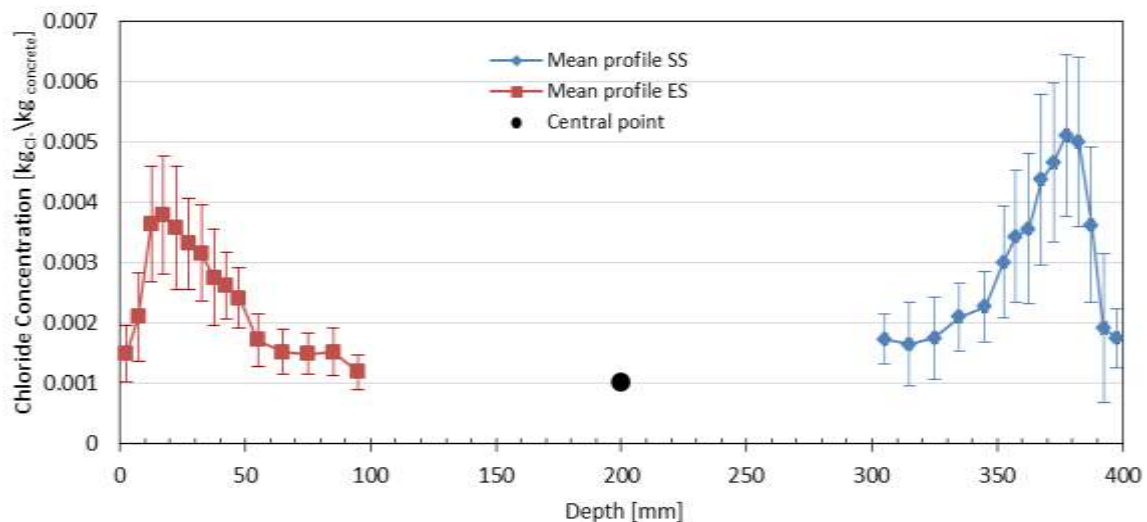
181  
 182 Fig. 3: Example of profiles with outliers (high values of concentration) with respect to the global mean profile

Table 3: Summary of the profiles obtained

Sample	Position (cm)	SS	ES	Sample	Position (cm)	SS	ES	Sample	Position (cm)	SS	ES
1	20	☒	☒	11	320	☐	☐	21	620	☒	☒
2	50	☒	☒	12	350	☐	☐	22	650	☒	☐
3	80	☐	☐	13	380	☒	☒	23	680	☒	☒
4	110	☒	☒	14	410	☒	☒	24	710	☒	☒
5	140	☒	☒	15	440	☐	☐	25	740	☒	☒

6	170	☒	☐	16	470	☒	☒	26	770	☐	☐
7	200	☒	☐	17	500	☐	☐	27	800	☒	☒
8	230	☒	☐	18	530	☒	☒	28	830	☒	☒
9	260	☐	☐	19	560	☒	☐	29	860	☐	☐
10	290	☒	☒	20	590	☐	☐	30	890	☒	☒

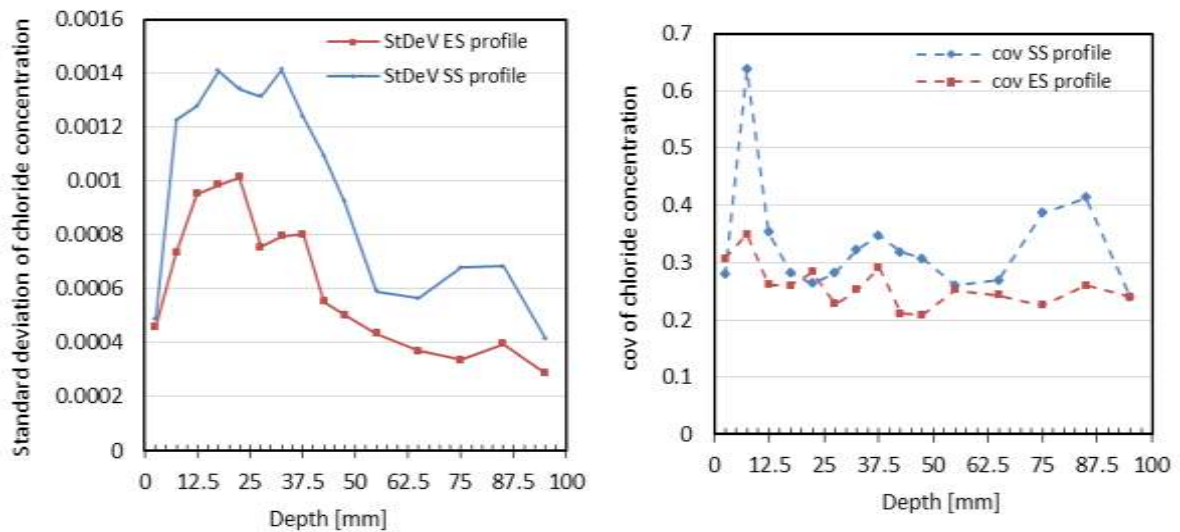
183 For the sake of clarity, only mean chloride ingress profiles and error bars corresponding to standard deviation are  
 184 presented in Fig. 4 for both exposures. The mean value is calculated for both sides from the retained  
 185 experimental profiles (21 and 16 profiles for SS and ES, respectively). It ought to be pointed out that the number  
 186 of profiles is very high and composes a substantial high value data base that can be used to estimate low order  
 187 statistics (mean and standard deviation) with a low statistical uncertainty. It should also be reminded here that all  
 188 the chloride profiles studied come from the same structure, with the same concrete material and the same  
 189 environmental conditions (constant height above sea level, orientation, exposure, etc.). However, despite this, all  
 190 the points of the profiles display a high standard deviation.



191 Fig. 4: Mean chloride profiles for both exposures (SS and ES) and for the central point (used as initial chloride  
 192 content)

193 The chloride profiles from both sides of the beam (SS and ES) reveal identical behaviour: first, a low chloride  
 194 content at the concrete surface, which increases to a peak value (around 20 mm for the mean profile) and then  
 195 decreases to the central point (estimated from eight samples and corresponding to slice n°3 on Fig. 2c). Then the  
 196 chloride profiles reveal the well-known bell shape as it appears in many researches (Song et al., 2008; Win et al.,  
 197 2004). It should also be noted that the standard deviation values are higher and more variable on the sheltered  
 198 side (Fig. 5a) and that they remain lower than 0.000156, the upper bound of the standard deviation of the error  
 199 on chloride measurements calculated by Bonnet et al. (2017). Moreover, the lower the chloride content, the

200 smaller the standard deviation. This observation may be accounted for by the fact that high chloride content is  
 201 affected by a combination of several factors, which are very changeable along the beam due to the environment  
 202 or to the heterogeneity of concrete during processing (vibration). The coefficient of variation is similar on both  
 203 sides with most values within the range 0.25-0.35, save near the beam surface (Fig. 5b). This confirms an  
 204 interesting statistical property for probabilistic modelling: the higher the chloride content, the higher the  
 205 uncertainty. Duprat (2007) has shown that a high degree of uncertainty combined with some environmental  
 206 parameters makes the chloride intake unpredictable. Chloride content values, on the other hand, are higher on the  
 207 sheltered side because the concrete beam stands in a confined environment, highly loaded with salt spray.  
 208 Chloride ions are trapped beneath the slab.



a)

b)

Fig. 5: a) Standard Deviation (StDev) and b) coefficient of variation (COV) for chloride content for both exposures

### 209 3.2. Analytical model for diffusion law

210 In a marine environment, concrete can be considered as almost saturated. Indeed, the concrete used for the  
 211 studied beam was casted in-situ. Thus, it was initially saturated and persistently exposed to high RH. RH,  
 212 superior to 80%, as shown in Table 2 was measured according to a national meteo station located nearby the  
 213 beam but not so closed to the sea water as this one. Moreover the beam is submitted to water coming from  
 214 splashing and/or rain. Besides, the pore network of the cement matrix is very thin. Baroghel-Bouny et al. (1999)  
 215 explained that in this case the water displacement into concrete is low and can be described by a diffusion  
 216 equation.

217 . Thus, chloride ingress is modelled using Fick's diffusion model except near the surface and it is applied to fit  
218 the experimental chloride profiles.

219 For a homogeneous concrete, a constant surface content and a one- dimensional diffusion into a semi-infinite  
220 space, Fick's second law is expressed as:

$$C(x, t) = C_0 + (C_s - C_0) \operatorname{erfc} \left( \frac{x}{2\sqrt{Dt}} \right) \quad (1)$$

221 where  $C$  is the chloride content at a depth of  $x$  (m) after time  $t$  (s);  $C_0$  ( $\text{kg}_{\text{Cl}}/\text{kg}_{\text{concrete}}$ ) the initial chloride content  
222 in concrete before exposure,  $C_s$  ( $\text{kg}_{\text{Cl}}/\text{kg}_{\text{concrete}}$ ) the chloride content at the surface and  $D$  ( $\text{m}^2/\text{s}$ ) the diffusion  
223 coefficient.

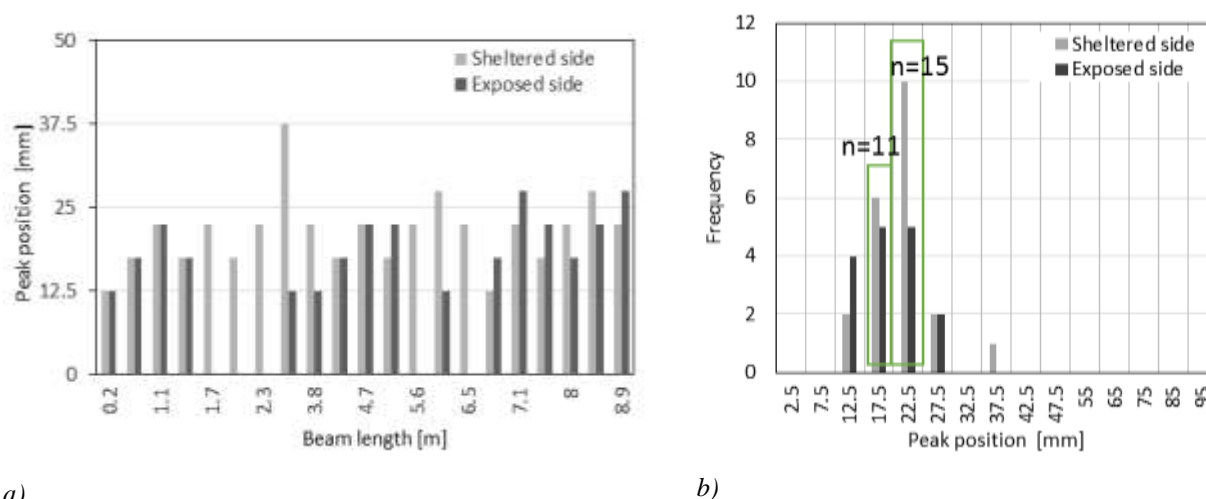
224 The initial chloride content  $C_0$  is obtained from eight samples at a depth of 200mm, which is considered distant  
225 enough from the surface to be representative of uncontaminated concrete. A very low negligible coefficient of  
226 variation (less than 2%) is obtained with a mean value  $C_0=0.001019 \text{ kg}_{\text{Cl}}/\text{kg}_{\text{concrete}}$ , a maximum value=  $0.001066$   
227  $\text{kg}_{\text{Cl}}/\text{kg}_{\text{concrete}}$  and a minimum value=  $0.000964 \text{ kg}_{\text{Cl}}/\text{kg}_{\text{concrete}}$ . The mean value is subsequently used. Besides  $C_s$   
228 and  $D$  are not time dependant in the paper, as it was done by (Chalee et al., 2009; Tadayon et al., 2016; Valipour  
229 et al., 2013), since all the samples have been taken from the same beam at the same age of 28 years old.  
230 Moreover it was shown by Ben Fraj et al. (2012) that the diffusion coefficient decreases particularly in the first  
231 few months. The values for  $C_s$  and  $D$  were provided simultaneously by fitting the experimental profiles with Eq.1  
232 and were obtained by iteration using the Mathematica software with the least square minimization method

### 233 3.3. Fitting method

234  $C_0$  being known, the estimation of parameters  $C_s$  and  $D$  of Fick's second law by fitting the experimental chloride  
235 profiles implies that these profiles have a monotonic decreasing shape. This is not, however, the case near the  
236 concrete surface where the first few centimetres present a high positive chloride gradient (Fig. 4). That is why  
237 discarding the first few centimetres below the surface is a commonly used technique (Chalee et al., 2009; Pang  
238 and Li, 2016). Da Costa et al. (2013) specify that the aim in doing this is to eliminate lixiviation effect.

239 Moreover, Fig. 6a shows that peak positions (the depth corresponding to the maximal chloride concentration)  
240 occurs at different depths between 12.5 mm and 37.5 mm with a maximum occurrence within the range 12.5 mm  
241 - 22.5 mm. The objective of the following section is to examine the effect of pre-treatment (discarding of  
242 experimental data close to the surface) on the estimation of the Fick's law parameters. We will compare some

243 generic treatments (Cases 2 and 3) commonly used in various research works with the individual treatment (Case  
 244 1), which is specific to each chloride profile; the objective is here to evaluate the relevance of the latter.



a) b)  
 Fig. 6: a) Distribution of peak positions (relative to the concrete surface) along the beam and b) Frequency of the peak positions

245 The three different experimental data pre-treatments studied here are now described:

246 - In the first case, called “reference case”, the treated profiles start from the real peak value that varies  
 247 from a sample to another (no assumption is required). This method, where the peak position is assumed to be a  
 248 random variable, is in better agreement with the real evolution of data. The trend, indeed, is a decreasing one  
 249 (Bastidas et al, 2011, Nilsson et al., 2010). The peak value position varies within the range 12.5 mm - 37.5 mm  
 250 (Fig. 6). The pre-treatment of the experimental profiles is then carried out on an individual basis.

251 The two other treatments can be carried out on a systematic basis, relying, however, on the assumption of the  
 252 peak position, which is assumed here to be deterministic:

253 - In the second case “15-mm discarded case”, all data from the first 15 mm below the concrete surface  
 254 are discarded. All the profiles start with the data at abscissa 17.5 mm, which corresponds to a recurrent  
 255 frequency peak depth for both exposed and sheltered sides (n=11 in Fig. 6b). Moreover, the maximum absolute  
 256 deviation between the real peak value (corresponding to the starting point in the reference case-1) and the value  
 257 at 17.5 mm is 0.0022 kg<sub>Cl</sub>/ kg<sub>concrete</sub> for the sheltered side and 0.0012 kg<sub>Cl</sub>/ kg<sub>concrete</sub> for the exposed side.

258 - In the third case “20-mm discarded case”, all data from the first 20 mm below the concrete surface are  
 259 discarded. The profiles here start at abscissa 22.5 mm, which is the highest peak position frequency for both the  
 260 sheltered and the exposed sides (n=15 for SS and 5 for ES in Fig. 6b). Moreover, the maximum absolute

261 deviation between the real peak value and the value at 22.5 mm is 0.0014 kg<sub>Cl</sub>/ kg<sub>concrete</sub> for the sheltered side  
262 and 0.0015 kg<sub>Cl</sub>/ kg<sub>concrete</sub> for the exposed side.

## 263 4. Results and discussion

### 264 4.1. Preliminary comparison of the three pre-treatments

265 The 37 experimental profiles are fitted using Fick's second law (Eq. 1) with the three pre-treatments to estimate  
266  $C_s$  and  $D$  parameters. The main trends emerging from the results are discussed on the basis of the study of three  
267 profiles. Fig. 7 illustrates the fitting for three profiles with different real peak positions: 12.5 mm (profile 1ES),  
268 17.5 mm (profile 14ES) and 22.5 mm. (profile 4ES). The analysis of the shape of the curves, which can indicate  
269 the trend for (i)  $C_s$  and (ii)  $D$ , is then conducted. The quantitative results are displayed in Table 4 where the  
270 relative error (RE) is defined as

$$\text{RE} = (y - y_{\text{ref}}) / y_{\text{ref}} \quad (2)$$

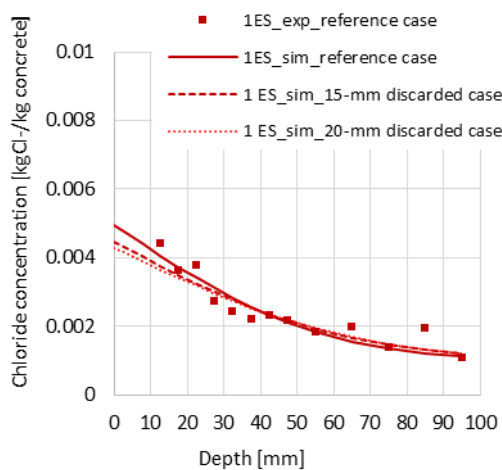
271 where  $y$  is  $C_s$  or  $D$  for the two pre-treatment cases (discarded 15 mm and 20 mm, respectively),  $y_{\text{ref}}$  is  $C_s$  or  $D$  for  
272 the reference case.

273 (i) The estimation of the surface chloride content is first examined. For most specimens, pre-treatments 2  
274 and 3 underestimate  $C_s$ . Moreover, the error is even greater when the real peak position at 22.5 mm is  
275 approximated by discarding the first 15mm (Fig. 7c). At this point, it can be concluded that the case where points  
276 situated before the real peak position are discarded, increases the error contrary to the case where they are  
277 discarded beyond the real peak position (Fig. 7a and Fig. 7b versus Fig. 7c)

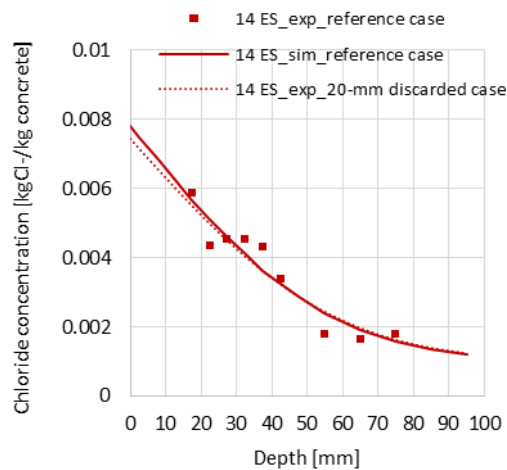
278 [Song et al. \(2008\)](#) give two reasons to explain the problem of the determination of  $C_s$ : first, the composition of  
279 the concrete skin may be different from that of concrete inside the structure and second, the effects of some  
280 phenomena like the reaction between the concrete surface and the surrounding environment. On this basis, it can  
281 be concluded that the individual treatment respects the chloride intake capacity for each sample/position.

282 (i) The diffusion coefficient estimation is then discussed because it is one of the main parameters for  
283 assessing material performances as regards chloride penetration (da Costa et al., 2013). For most specimens here  
284 also, pre-treatments 2 and 3 overestimate  $D$  with a significant relative error. The result is a shortened predicted  
285 service life and increased maintenance costs (Bastidas and Schoefs, 2012) because of early scheduled repair  
286 operations.

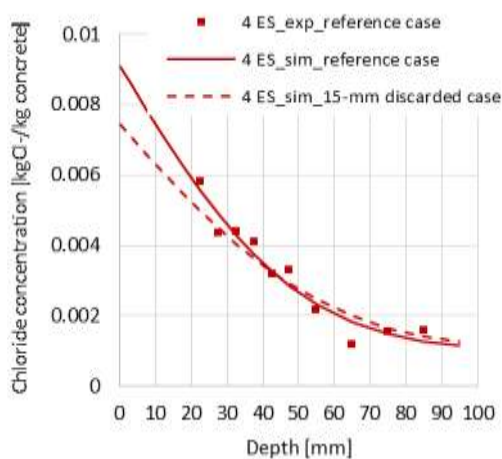
287 The comparison of the three pre-treatment cases is applied to all the profiles (37 profiles). The conclusions are  
 288 the same as those obtained for ES profiles 1, 4 and 14. The overall detail of the results is presented in Section  
 289 4.3.



a)



b)



c)

Fig. 7: Fitting model results for chloride profiles showing a peak at a) 12.5 mm (sample 1ES), b) 17.5 mm (sample 14ES), and c) 22.5 mm (sample 4ES)

Table 4: Estimated values of  $C_s$  (kg Cl-/kg concrete) and relative error (RE) with the reference case for profiles 1,4 and 14

	Peak at 12.5 mm		Peak at 17.5 mm		Peak at 22.5 mm	
	Fig. 7a		Fig. 7b		Fig. 7c	
	$C_s$	RE	$C_s$	RE	$C_s$	RE
<i>Reference case</i>	0.00495	0%	0.00779	0%	0.00908	0%
15-mm discarded case	0.00446	9.9%	0.00779	0%	0.00742	18.3%
20-mm discarded case	0.00428	13.4%	0.00743	4.5%	0.00908	0%

Table 5: Estimated values of  $D$  ( $10^{-12}$  m<sup>2</sup>/s) and relative error (RE) with the reference case for profiles 1,4 and 14

	Peak at 12.5 mm	Peak at 17.5 mm	Peak at 22.5 mm
--	-----------------	-----------------	-----------------

	<i>D</i>	RE	<i>D</i>	RE	<i>D</i>	RE
<i>Reference case</i>	1.08	0%	1.06	0%	0.87	0%
15-mm discarded case	1.36	25.4%	1.06	0%	1.17	33.7%
20-mm discarded case	1.48	36.1%	1.14	7.6%	0.87	0%

290 4.2. Effects on peak position

291 In order to quantify the sensitivity of  $C_s$  and  $D$  to treatment methods, the relative error (Eq. 2) is plotted vs. the  
292 distance to the peak position  $N_x$  (Eq. 3).

$$N_x = x - x_{ref} \quad (3)$$

293 where,  $x$  is the depth as displayed in Fig. 6b ( $x$  takes the value 17.5 mm for the '15-mm discarded' case and 22.5  
294 mm for the "20-mm discarded case" and  $x_{ref}$  is the real abscissa of the peak (reference case).

295 If  $N_x > 0$ , the real peak position is closer to the surface than 17.5 mm (case 2) or 22.5 mm (case 3). Otherwise  
296 ( $N_x < 0$ ), the peak occurs deeper than 17.5 mm or 22.5 mm.

297 Fig. 8 shows that when  $N_x > 0$ , the values of  $C_s$  are underestimated by 60% when the overestimation of  $D$  is 2  
298 times greater. A similar trend is observed when  $N_x < 0$ . In other words,  $C_s$  is underestimated when  $D$  is  
299 overestimated.

300 Those results highlight the significant effect of the mathematical expression of the model on the assessment of  
301 the estimated parameters  $C_s$  and  $D$ .

302 This affects the prediction of maintenance and repair operations: surface chloride content represents the extent of  
303 the aggressive action of a marine environment on concrete structures and provides an important boundary  
304 condition for service life prediction and quantitative durability design of RC structures.

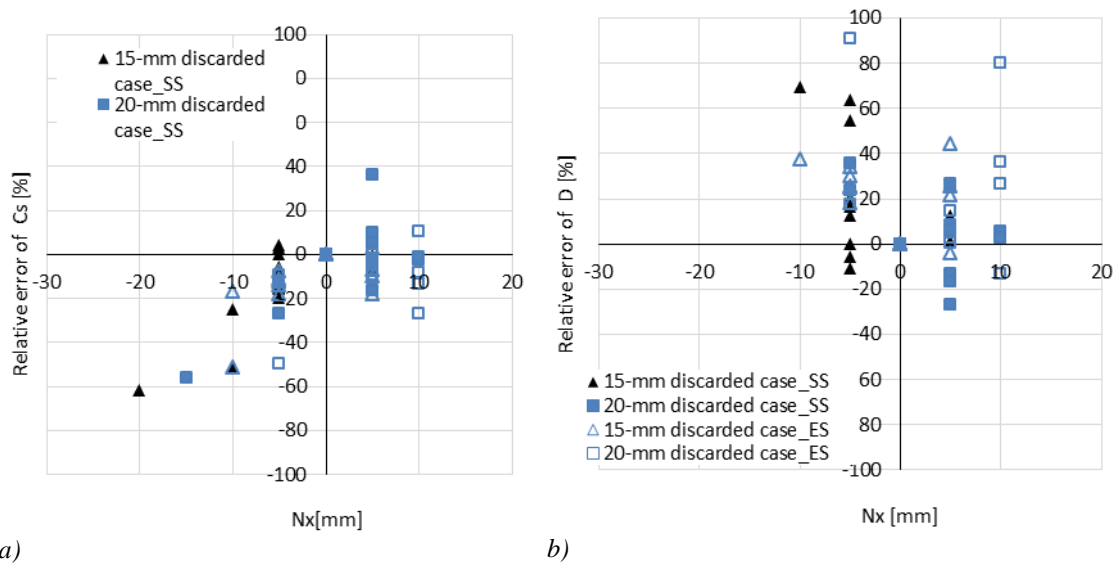


Fig. 8: Relative error vs.  $N_x$  for a)  $C_s$  and b)  $D$

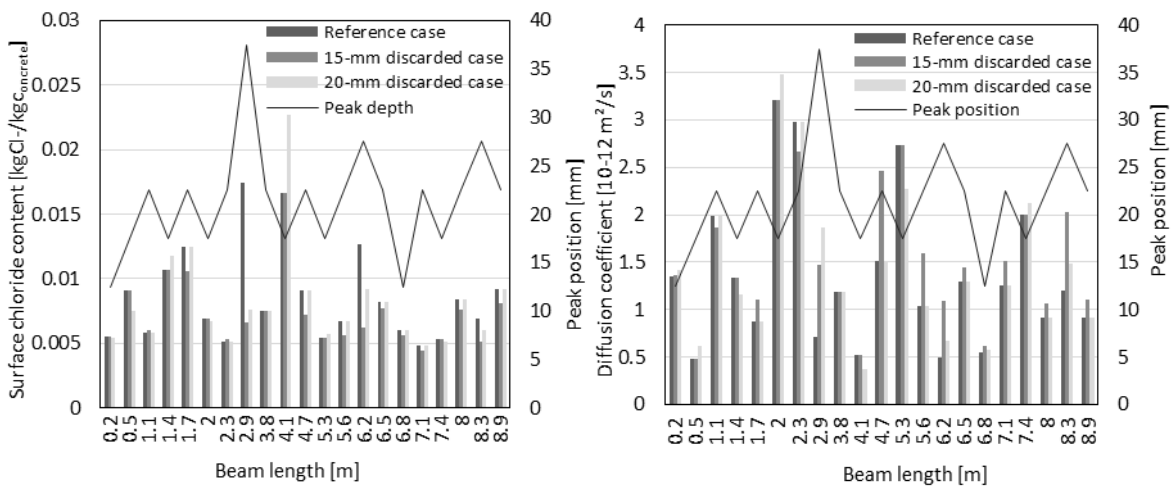
#### 4.3. Comparison of the estimated mean and standard deviations for $C_s$ and $D$ on the whole data base

The previous section underlined the effect of an individual pre-treatment of the experimental chloride profiles (reference case) on the relative error. In this section, a quantitative analysis is carried out to highlight the impact of pre-treatment on the mean and standard deviations of the estimated parameters. The values of the chloride surface contents and diffusion coefficients along the beam, estimated using the three pre-treatment methods, are given in Fig. 9. The real position of the peak is also plotted on the same figure (solid line). The scatter of the points is more pronounced on the sheltered side and will be exhaustively discussed below. It should be noted that, from a statistical point of view, this could be partly related to the number of points used to fit the experimental chloride profiles. All the curves have 12 points each (starting from 2.5 mm to 95 mm). However, when the peak occurs deep from the surface (deeper than 22.5 mm), few points only remain for fitting. For the 15-mm and 20-mm discarded cases, the number of points is 12 and 11, respectively.

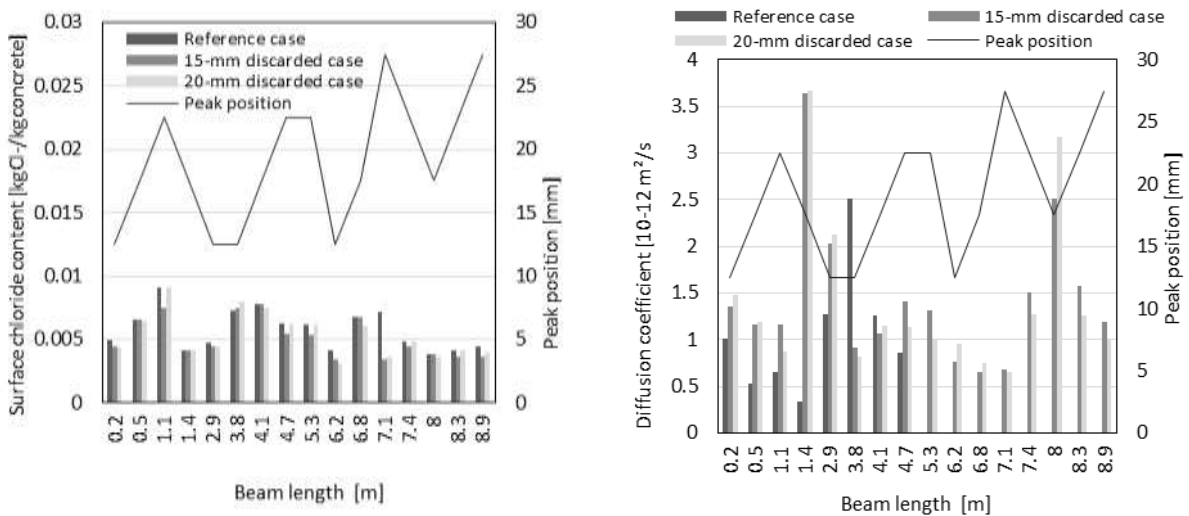
$C_s$  is first examined for both exposures (Fig. 9a, right side and Fig. 9b, left side). Most of  $C_s$  values are coherent between the different treatments for both exposures. Moreover, the trend observed in the previous section is confirmed: the deeper the peak, the higher the error is (unde-estimation) when discarding points before 15 mm. We observe that the peak occurs principally at 22.5 mm for the sheltered side (10 profiles / total of 21 profiles-SS but only on five profiles for the exposed side (total of 16 profiles-ES). The total mean value of  $C_s$  on the sheltered side is  $0.00802 \text{ kg}_{\text{Cl}}/\text{kg}_{\text{concrete}}$  (min =  $0.00731 \text{ kg}_{\text{Cl}}/\text{kg}_{\text{concrete}}$ ; max =  $0.00856 \text{ kg}_{\text{Cl}}/\text{kg}_{\text{concrete}}$ ) whereas the mean value of  $C_s$  on the exposed side is  $0.0054 \text{ kg}_{\text{Cl}}/\text{kg}_{\text{concrete}}$  (min =  $0.00514 \text{ kg}_{\text{Cl}}/\text{kg}_{\text{concrete}}$ ; max =  $0.00576 \text{ kg}_{\text{Cl}}/\text{kg}_{\text{concrete}}$ ). The values obtained are in accordance with those found in the literature for real structures in a

324 marine environment with comparable exposures and investigation periods:  $C_s$  can vary between 0.002 kg  $Cl^-$ /kg  
 325 concrete (33-year-old bridge- Table 1) (de Rincón et al., 2004) and 0.0078 kg  $Cl^-$ /kg concrete (29-year-old offshore  
 326 platform) (Medeiros-Junior et al., 2015).

327 Fig. 10 presents the mean values of  $C_s$  (as histograms) and the standard deviation: both are higher on the  
 328 sheltered side than on the exposed side. The sheltered side refers to a confined environment with high relative  
 329 humidity, which is more affected by sea water through splashing. Consequently, more spray is trapped under the  
 330 beam relative to the exposed side, which is more subjected to weather variations. This is in accordance with  
 331 Kenshel (2009) who explains the higher surface content values of  $C_s$  on the sheltered side up to three times by  
 332 the wash-down conditions due to driving rain on the exposed side.



a) sheltered side



b) exposed side

Fig. 9: Variation of  $C_s$  and  $D$  together with peak position (black curve) according to the set of analysis for a) the sheltered side and b) the exposed side

333 The estimated values of  $D$  for both exposures are then analysed (Fig. 9a and Fig. 9b- right side). The global  
 334 mean value of  $D$  is  $1.45 \times 10^{-12} \pm 7.9 \times 10^{-13}$  m<sup>2</sup>/s. Mean values are virtually the same for both sides of the beam  
 335 (Fig. 10) and in accordance with those found in the literature for real structures in a marine environment:  $D$  can  
 336 vary between  $2.75 \times 10^{-13}$  m<sup>2</sup>/s (case of a 25-year-old offshore platform-Table 1) (da Costa et al., 2013) and  
 337  $5.13 \times 10^{-12}$  m<sup>2</sup>/s (case of a 29-year-old offshore platform-Table 1) (Medeiros-Junior et al., 2015).  
 338 Again the importance of considering the real shape of the chloride profile with the real peak position must be  
 339 pointed out. This allows more efficient determination of  $C_s$  and  $D$ . These two deterioration parameters are the  
 340 most significant as regards the initiation stage of structure service life as shown by (Kenshel, 2009).

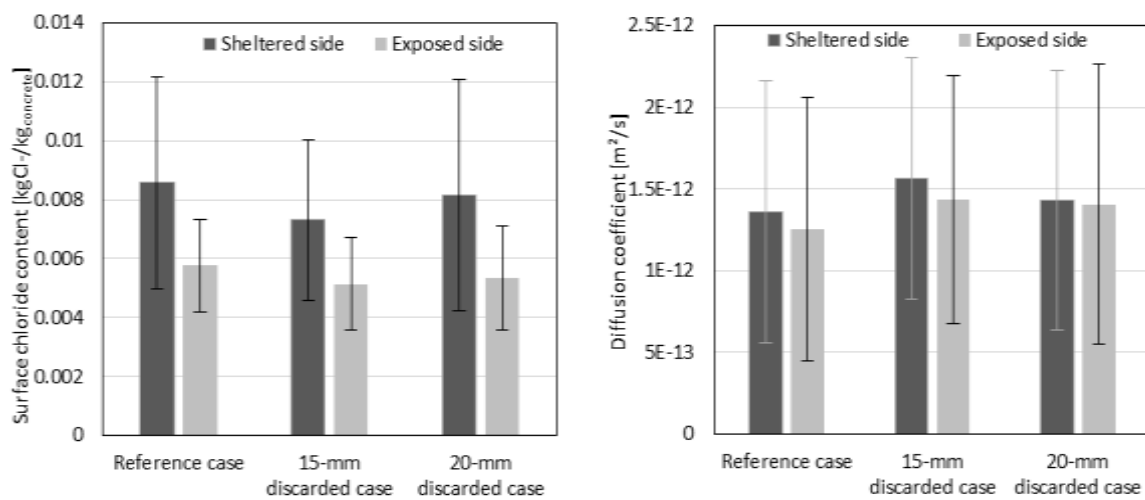


Fig. 10: Mean values (histograms) and standard deviations (error bars) for  $C_s$  and  $D$  for both exposures

#### 341 4.4. Statistical analysis for the reference case

342 The previous section underlined the need for an individual pre-treatment of the experimental chloride profiles  
 343 (reference case). The present section, therefore, focuses on the reference case with the aim of producing a model  
 344 for the estimated parameters of the Fick's diffusion model: 37 identified coefficients of  $C_s$  and  $D$  are available  
 345 when combining sheltered and exposed side results. The scatter of points for  $D$  and  $C_s$  is assessed by computing  
 346 their Coefficients of Variation (CoV) (Table 6):  $D$  scattering is larger (CoV( $D$ )=0.61) than  $C_s$  one (CoV( $C_s$ )=  
 347 0.44), an expected result in view of Fig. 10 analysis. Moreover, those values are consistent with the data found in  
 348 the literature: CoV( $D$ ) ranges from 0.38 to 0.69 and CoV( $C_s$ ) ranges from 0.31 to 0.83 (Table 6).

Table 6: Comparison between values found in the literature and experimental values of CoV (%) for  $C_s$  and  $D$

	$C_s$	$D$
Kenshel (2009)	56	40
Pang and Li (2016)	55	69
Berke and Hicks (1992) [ref (Kenshel, 2009)]	40	-

Wood and Crerar (1997) [ref (Duprat, 2007) ]	63	38
Uji et al. (1990) [ref (Duprat, 2007) ]	83	-
Cramer et al. (2002)	51	57
Pritzl et al. (2015)	31	42
<b>Actual Study</b>	SS	42
	ES	27
	Global (mean of SS and ES)	44

349 It clearly appears that these parameters should be modelled by random variables. Fig.8 has shown that  $D$  and  $C_s$   
350 are not independent because they come both from the regression of the chloride profile using Fick's 2<sup>nd</sup> law.  
351 Further  $C_s$  does not come from a direct measurement on the concrete surface but it comes rather from an  
352 extrapolation of chlorides in the material (starting from 7.5 mm to 37.5 mm as shown in fig 6) to the abscissa  
353  $x=0$  mm.

354 We now examine their statistical dependence by plotting the scatter diagram of  $C_s$  and  $D$  in Fig. 11. It can be  
355 noticed that, whatever the exposure, for a tight range of  $C_s$  (around 0.004 kg<sub>Cl</sub>/kg<sub>concrete</sub>),  $D$  ranges from  
356  $0.36 \times 10^{-12}$  to  $3.67 \times 10^{-12}$  m<sup>2</sup>/s. This trend clearly demonstrates that  $C_s$  and  $D$  are correlated when identified from  
357 Fick's 2<sup>nd</sup> law. Conversely, a joint distribution of these parameters should be used when modeling  $C_s$  and  $D$  as  
358 random variables and propagating uncertainties through the same model. However, this rule is not general. Note  
359 that physically,  $C_s$  depends not only on the environmental conditions but also on the composition of concrete due  
360 to the chloride fixation capacity of the binder, which in turn depends on its free chloride content and so on its  
361 diffusivity. Indeed  $C_s$  is determined by fitting and using the experimental chloride contents close to the surface.  
362 However until now, no data are available and our proposition is only valuable for Fick's second law model.

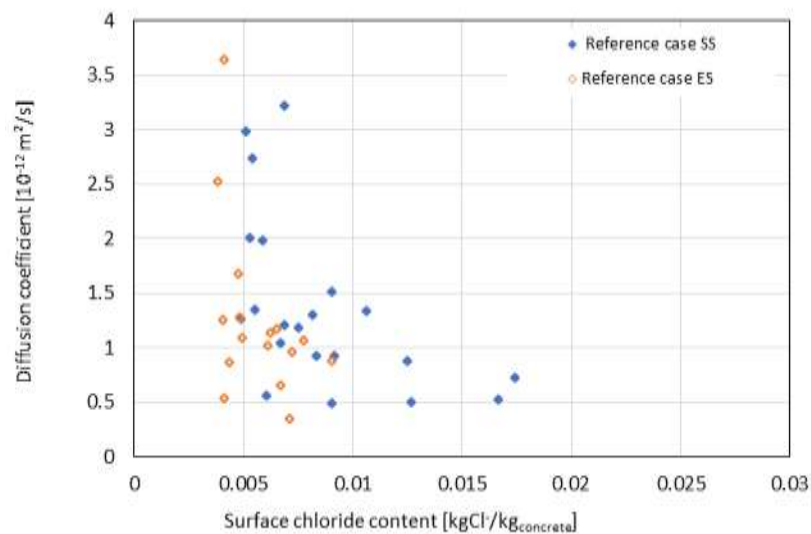


Fig. 11:  $C_s$  and  $D$  scatter diagram for the both exposures (reference case)

363 Probabilistic modelling last key step consists in the assessment of marginal probability density functions (pdf).  
 364 The probabilistic distribution and fitting with a lognormal pdf according to the maximum likelihood estimate are  
 365 plotted in Fig. 12. As suggested in the literature,  $C_s$  and  $D$  are well fitted by a lognormal pdf (Duprat, 2007; Li et  
 366 al., 2015). The lognormal parameters used in this study are given in Fig. 12. Applying a lognormal pdf for the  
 367 results obtained appears relevant because both parameters are positive. Moreover, their distribution is  
 368 dissymmetric as shown in Fig. 12.

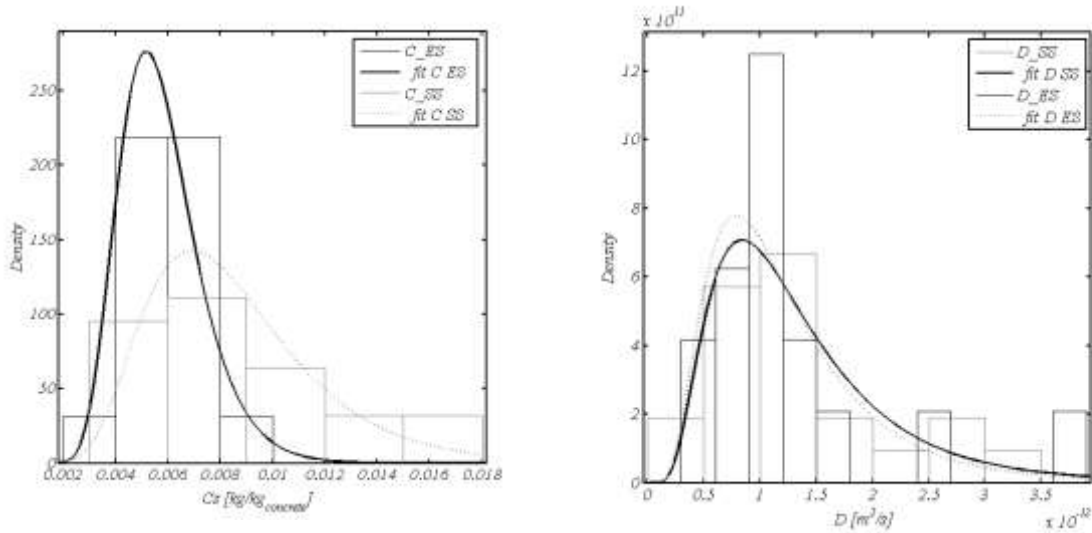


Fig. 12: Lognormal pdf of  $C_s$  and  $D$  for the reference case

369 Table 7: Lognormal pdf parameters for  $C_s$  and  $D$  (reference case)

	$C_s$ (kgCl/kg concrete)		$D$ (m <sup>2</sup> /s)		370
	$\mu$	$\sigma$	$\mu$	$\sigma$	371
Sheltered side	0.0085	$1.1210^{-5}$	$1.3710^{-12}$	$7.19 \cdot 10^{-3}$	372 The Table 7
Exposed side	0.0057	$2.510^{-6}$	$1.2510^{-12}$	$5.72 \cdot 10^{-3}$	373 points out that

374 the mean value of  $C_s$  on the sheltered side is 1.5 times higher than on the exposed side. This result is in  
 375 accordance with the global observations conducted on the field data in Fig. 4 and with the results obtained by  
 376 Kenshel (2009) where  $C_s$  is up to three times higher on the north side than on the south side with regard to the  
 377 prevailing wind.

### 378 5. Conclusion

379 The present study has been conducted to examine a 28-year-old reinforced concrete structure in a marine splash  
 380 zone. An important set of chloride data is studied, which constitutes a substantial material for spatial variability  
 381 modelling. Chloride profiles have been measured every 30 cm on the same beam line with two different  
 382 exposure situations: a sheltered side (SS) and an exposed side (ES).

383 The following conclusions can be drawn:

- 384 - 37 workable chloride profiles (21 for SS and 16 for ES) collected along a beam located in an  
385 estuary area are studied. Chloride content values are higher on the sheltered side. This can be  
386 explained by the fact that the sheltered side is also the lee side and is highly moisture laden. On this  
387 side, saline spray is trapped and the contact with seawater is greater due to splashing.
- 388 - The experimental chloride profiles are fitted using Fick's second law in order to estimate its  
389 parameters: the surface content  $C_s$  and the diffusion coefficient  $D$ . Three pre-treatments of these  
390 profiles are carried out: a "reference case" (individual treatment), a "15-mm discarded" case and a  
391 "20-mm discarded" case (generic treatments). The reference case results underline the sensitivity of  
392 the parameters to the first point corresponding to the maximum content position. When a generic  
393 method is applied (systematic discarding of the first few millimetres below the surface), as is the  
394 case in the literature,  $C_s$  is underestimated whereas  $D$  is overestimated. Consequently, the rate of  
395 error relating to the reference case is around 50% for  $C_s$  and can reach 100% for  $D$ .
- 396 - The reference case is used for the statistical study. The computation of the coefficient of variation  
397 reveals that  $D$  scattering is larger (CoV= 59% for SS and CoV=64% for ES) than  $C_s$  one (CoV=  
398 42% for SS and CoV= 27% for ES) and that their values are consistent with the data found in the  
399 literature. Moreover, the global mean value of  $C_s$  is 0.7%  $\text{kg}_{\text{Cl}^-}/\text{kg}_{\text{concrete}}$  (calculated for both  
400 sheltered and exposed sides) and corresponds to a certain risk of corrosion according to the risk  
401 classification proposed by Bamforth (Bamforth, 1996)
- 402 - Finally  $C_s$  and  $D$  have a dissymmetric distribution and are well fitted with a lognormal distribution.

403 These results underline the importance of the individual treatment of field chloride profiles for an accurate  
404 determination of  $C_s$  and  $D$ . Reducing uncertainties of those key parameters inputs for corrosion damage detection  
405 allows the development of a probabilistic-based performance prediction tool that can be used to predict  
406 accurately the time to corrosion initiation and hence the optimal time for repair/maintenance intervention of  
407 reinforced concrete structures in a marine environment. Furthermore as the chloride profiles are made from a  
408 destructive method which is a tedious procedure, it is interesting for the owner to optimize the number of cores.  
409 This study done on 30 profiles extracted at a distance of 30 cm from each other would allow optimizing the  
410 number of coring.

411

412 **Acknowledgment**

413 The authors would like to acknowledge and thank the harbour of Nantes-Saint Nazaire "Grand Port de Nantes  
414 Saint Nazaire", especially Mr. Laurent Suire and Mr. Pascal Lijours, for supporting this study, and Mr. Michel  
415 Roche for his technical support

416 **References**

- 417 Andrade, C., Diez, J.M., Alonso, C., 1997. Mathematical Modeling of a Concrete Surface "Skin Effect" on  
418 Diffusion in Chloride Contaminated Media. *Advanced Cement Based Materials* 6, 39–44.  
419 [https://doi.org/10.1016/S1065-7355\(97\)00002-3](https://doi.org/10.1016/S1065-7355(97)00002-3)
- 420 Bamforth, P.B., 1996. Definition of exposure classes and concrete mix requirements - Technische  
421 Informationsbibliothek (TIB), in: *Corrosion of Reinforcement in Concrete Construction*. Presented at  
422 the International symposium; 4th, Corrosion of reinforcement in concrete construction, Cambridge, pp.  
423 176–190.
- 424 Baroghel-Bouny, V., Mainguy, M., Lassabatere, T., Coussy, O., 1999. Characterization and identification of  
425 equilibrium and transfer moisture properties for ordinary and high-performance cementitious materials.  
426 *Cement and Concrete Research* 29, 1225–1238. [https://doi.org/10.1016/S0008-8846\(99\)00102-7](https://doi.org/10.1016/S0008-8846(99)00102-7)
- 427 Bastidas-Arteaga, E., Chateauneuf, A., Sánchez-Silva, M., Bressolette, P., Schoefs, F., 2011. A comprehensive  
428 probabilistic model of chloride ingress in unsaturated concrete. *Engineering Structures* 33, 720–730.  
429 <https://doi.org/10.1016/j.engstruct.2010.11.008>
- 430 Ben Fraj, A., Bonnet, S., Khelidj, A., 2012. New approach for coupled chloride/moisture transport in non-  
431 saturated concrete with and without slag. *Construction and Building Materials* 35, 761–771.  
432 <https://doi.org/10.1016/j.conbuildmat.2012.04.106>
- 433 Berke, N.S., Hicks, M.C., 1992. Estimating the Life Cycle of Reinforced Concrete Decks and Marine Piles  
434 Using Laboratory Diffusion and Corrosion Data. <https://doi.org/10.1520/STP19764S>
- 435 Bonnet, S., Schoefs, F., salta, M., 2017. Sources of uncertainties for total chloride profile measurements in  
436 concrete: quantization and impact on probability assessment of corrosion initiation. *European Journal of*  
437 *Environmental and Civil Engineering*. <https://doi.org/doi.org/10.1080/19648189.2017.1375997>
- 438 Chalee, W., Jaturapitakkul, C., Chindaprasirt, P., 2009. Predicting the chloride penetration of fly ash concrete in  
439 seawater. *Marine Structures* 22, 341–353. <https://doi.org/10.1016/j.marstruc.2008.12.001>
- 440 Chaussadent, T., Arliguie, G., 1999. AFREM test procedures concerning chlorides in concrete: Extraction and  
441 titration methods. *Mat. Struct.* 32, 230–234. <https://doi.org/10.1007/BF02481520>
- 442 Cramer, S.D., Covino Jr., B.S., Bullard, S.J., Holcomb, G.R., Russell, J.H., Nelson, F.J., Laylor, H.M., Soltesz,  
443 S.M., 2002. Corrosion prevention and remediation strategies for reinforced concrete coastal bridges.  
444 *Cement and Concrete Composites, CORROSION AND CORROSION MONITORING* 24, 101–117.  
445 [https://doi.org/10.1016/S0958-9465\(01\)00031-2](https://doi.org/10.1016/S0958-9465(01)00031-2)
- 446 da Costa, A., Fenaux, M., Fernández, J., Sánchez, E., Moragues, A., 2013. Modelling of chloride penetration into  
447 non-saturated concrete: Case study application for real marine offshore structures. *Construction and*  
448 *Building Materials* 43, 217–224. <https://doi.org/10.1016/j.conbuildmat.2013.02.009>
- 449 de Rincón, O.T., Castro, P., Moreno, E.I., Torres-Acosta, A.A., de Bravo, O.M., Arrieta, I., García, C., García,  
450 D., Martínez-Madrid, M., 2004. Chloride profiles in two marine structures—meaning and some  
451 predictions. *Building and Environment* 39, 1065–1070. <https://doi.org/10.1016/j.buildenv.2004.01.036>
- 452 de Vera G., Climent M. A., Viqueira E., Antón C., López M. P., 2015. Chloride Penetration Prediction in  
453 Concrete through an Empirical Model Based on Constant Flux Diffusion. *Journal of Materials in Civil*  
454 *Engineering* 27, 04014231. [https://doi.org/10.1061/\(ASCE\)MT.1943-5533.0001173](https://doi.org/10.1061/(ASCE)MT.1943-5533.0001173)
- 455 Duprat, F., 2007. Reliability of RC beams under chloride-ingress. *Construction and Building Materials* 21,  
456 1605–1616. <https://doi.org/10.1016/j.conbuildmat.2006.08.002>
- 457 Fédération International du Béton, 2006. Model code for service life design. Bulletin 34. Lausanne:fib.

458 Guo, A., Li, H., Ba, X., Guan, X., Li, H., 2015. Experimental investigation on the cyclic performance of  
459 reinforced concrete piers with chloride-induced corrosion in marine environment. *Engineering*  
460 *Structures* 105, 1–11. <https://doi.org/10.1016/j.engstruct.2015.09.031>

461 Hilsdorf, H., Kropp, J., 2004. *Performance Criteria for Concrete Durability*. CRC Press.

462 Kenshel, O.M., 2009. *Influence on Spatial Variability on Whole Life Management of Reinforced Concrete*  
463 *Bridges*. Trinity College.

464 Li, J., Shao, W., 2014. The effect of chloride binding on the predicted service life of RC pipe piles exposed to  
465 marine environments. *Ocean Engineering* 88, 55–62. <https://doi.org/10.1016/j.oceaneng.2014.06.021>

466 Li, Q., Li, K., Zhou, X., Zhang, Q., Fan, Z., 2015. Model-based durability design of concrete structures in Hong  
467 Kong–Zhuhai–Macau sea link project. *Structural Safety* 53, 1–12.  
468 <https://doi.org/10.1016/j.strusafe.2014.11.002>

469 Li, Q., Rao, J., Fazio, P., 2009. Development of {HAM} tool for building envelope analysis. *Building and*  
470 *Environment* 44, 1065–1073. <http://dx.doi.org/10.1016/j.buildenv.2008.07.017>

471 Luping, T., Gulikers, J., 2007. On the mathematics of time-dependent apparent chloride diffusion coefficient in  
472 concrete. *Cement and Concrete Research* 37, 589–595. <https://doi.org/10.1016/j.cemconres.2007.01.006>

473 Mangat, P.S., Molloy, B.T., 1994. Prediction of long term chloride concentration in concrete. *Materials and*  
474 *Structures* 27, 338–346. <https://doi.org/10.1007/BF02473426>

475 Medeiros-Junior, R.A. de, Lima, M.G. de, Brito, P.C. de, Medeiros, M.H.F. de, 2015. Chloride penetration into  
476 concrete in an offshore platform-analysis of exposure conditions. *Ocean Engineering* 103, 78–87.  
477 <https://doi.org/10.1016/j.oceaneng.2015.04.079>

478 Nguyen, P.T., Bastidas-Arteaga, E., Amiri, O., Soueidy, C.-P.E., 2017. An Efficient Chloride Ingress Model for  
479 Long-Term Lifetime Assessment of Reinforced Concrete Structures Under Realistic Climate and  
480 Exposure Conditions. *Int J Concr Struct Mater* 11, 199–213. <https://doi.org/10.1007/s40069-017-0185-8>

481 O’Connor, A.J., Kenshel, O., 2013. Experimental Evaluation of the Scale of Fluctuation for Spatial Variability  
482 Modeling of Chloride-Induced Reinforced Concrete Corrosion. *Journal of Bridge Engineering* 18, 3–14.  
483 [https://doi.org/10.1061/\(ASCE\)BE.1943-5592.0000370](https://doi.org/10.1061/(ASCE)BE.1943-5592.0000370)

484 Pang, L., Li, Q., 2016. Service life prediction of RC structures in marine environment using long term chloride  
485 ingress data: Comparison between exposure trials and real structure surveys. *Construction and Building*  
486 *Materials* 113, 979–987. <https://doi.org/10.1016/j.conbuildmat.2016.03.156>

487 Pritzl, M.D., Tabatabai, H., Ghorbanpoor, A., 2015. Long-term chloride profiles in bridge decks treated with  
488 penetrating sealer or corrosion inhibitors. *Construction and Building Materials* 101, Part 1, 1037–1046.  
489 <https://doi.org/10.1016/j.conbuildmat.2015.10.158>

490 Recommendation for analysis of total chloride in concrete., 2006. . *Materials and Structures* 35, 583–585.

491 Song, H.-W., Lee, C.-H., Ann, K.Y., 2008. Factors influencing chloride transport in concrete structures exposed  
492 to marine environments. *Cement and Concrete Composites* 30, 113–121.  
493 <https://doi.org/10.1016/j.cemconcomp.2007.09.005>

494 Tadayon, M.H., Shekarchi, M., Tadayon, M., 2016. Long-term field study of chloride ingress in concretes  
495 containing pozzolans exposed to severe marine tidal zone. *Construction and Building Materials* 123,  
496 611–616. <https://doi.org/10.1016/j.conbuildmat.2016.07.074>

497 Thomas, M.D.A., Matthews, J.D., 2004. Performance of pfa concrete in a marine environment—10-year results.  
498 *Cement and Concrete Composites* 26, 5–20. [https://doi.org/10.1016/S0958-9465\(02\)00117-8](https://doi.org/10.1016/S0958-9465(02)00117-8)

499 Uji, K., Matsuoka, Y., Maruya, T., 1990. Formulation of an equation for surface chloride content of concrete due  
500 to permeation of chloride. *Corrosion of reinforcement in concrete*. Papers presented at the third  
501 international symposium on “corrosion of reinforcement in concrete construction”, belfry hotel,  
502 wishaw, warwickshire, MAY 21–24, 1990. Publication of: CICC Publications.

503 Valipour, M., Pargar, F., Shekarchi, M., Khani, S., Moradian, M., 2013. In situ study of chloride ingress in  
504 concretes containing natural zeolite, metakaolin and silica fume exposed to various exposure conditions  
505 in a harsh marine environment. *Construction and Building Materials* 46, 63–70.  
506 <https://doi.org/10.1016/j.conbuildmat.2013.03.026>

- 507 Vennesland, P. by Ø., Climent, M.A., Andrade)\*\*\*, C.A.R.T.C. 178-T. (Carmen, 2012. Recommendation of  
508 RILEM TC 178-TMC: Testing and modelling chloride penetration in concrete\*. Materials and  
509 Structures 46, 337–344. <https://doi.org/10.1617/s11527-012-9968-1>
- 510 Wang, H.-L., Dai, J.-G., Sun, X.-Y., Zhang, X.-L., 2016. Characteristics of concrete cracks and their influence  
511 on chloride penetration. Construction and Building Materials 107, 216–225.  
512 <https://doi.org/10.1016/j.conbuildmat.2016.01.002>
- 513 Win, P.P., Watanabe, M., Machida, A., 2004. Penetration profile of chloride ion in cracked reinforced concrete.  
514 Cement and Concrete Research 34, 1073–1079. <https://doi.org/10.1016/j.cemconres.2003.11.020>
- 515 Wood, J.G.M., Crerar, J., 1997. Tay road bridge: Analysis of chloride ingress variability & prediction of long  
516 term deterioration. Construction and Building Materials, Corrosion and Treatment of Reinforced  
517 Concrete 11, 249–254. [https://doi.org/10.1016/S0950-0618\(97\)00044-5](https://doi.org/10.1016/S0950-0618(97)00044-5)
- 518